HDAC inhibitor ameliorates behavioral deficits in Mecp2308/y mouse model of Rett syndrome

Nicolas Lebrun, Chloé Delépine, Mohamed Selloum, Hamid Meziane, Juliette Nectoux, Yann Herault, Thierry Bienvenu

HDAC inhibitor ameliorates behavioral deficits in Mecp2 $^{308/y}$ mouse model of Rett syndrome

Nicolas Lebrun [a] , Chloé Delépine [b-e], Mohamed Selloum [f-j], Hamid Meziane [f-j], Juliette Nectoux [k], Yann Herault [f-j] and Thierry Bienvenu [a,d,k,*]

[a] INSERM U1266, Institut de Psychiatrie et de Neurosciences de Paris (IPNP), Paris, France

[b] INSERM, U1016, Institut Cochin, Paris, France.

[c] CNRS, UMR8104, Paris, France.

[d] Université de Paris, France.

[e] Massachusetts Institute of Technology, Department of Brain and Cognitive Sciences, Picower Institute for Learning and Memory, Cambridge, MA, USA

[f] Celphedia, PHENOMIN, Institut Clinique de la Souris (ICS), GIE CERBM, Illkirch, France

[g] Institut de Génétique et de Biologie Moléculaire et Cellulaire, Illkirch, France

[h] Centre National de la Recherche Scientifique, UMR7104, Illkirch, France

[i] Institut National de la Santé et de la Recherche Médicale, U964, Illkirch, France

[j] Université de Strasbourg, Illkirch, France

[k] Laboratoire de Génétique et de Biologie Moléculaires, APHP. Centre Université de Paris, France.

Running Title: HDAC inhibitor as emerging drug in Rett syndrome treatment

***Corresponding author**

Pr Thierry Bienvenu

Correspondence should be addressed to Pr. Thierry Bienvenu, Institut de Psychiatrie et de Neurosciences de Paris (IPNP), 102 rue de la Santé, 75014 Paris, France ; Email : thierry.bienvenu@inserm.fr. Phone : 01 58 41 16 17.

ABSTRACT

Rett syndrome (RTT) is a rare X-linked neurodevelopmental disorder. More than 95% of classic RETT syndrome cases result from pathogenic variants in the methyl-CpG binding protein 2 (*MECP2*) gene. Nevertheless, it has been established that a spectrum of neuropsychiatric phenotypes is associated with *MECP2* variants in both females and males. We previously reported that microtubule growth velocity and vesicle transport directionality are altered in *Mecp2*-deficient astrocytes from newborn *Mecp2*-deficient mice compared to that of their wild-type littermates suggesting deficit in microtubule dynamics. In this study, we report that administration of tubastatin A, a selective HDAC6 inhibitor, restored microtubule dynamics in *Mecp2*-deficient astrocytes. We furthermore report that daily doses of tubastatin A reversed early impaired exploratory behavior in male *Mecp2* $^{308/y}$ mice. These findings are a first step toward the validation of a novel treatment for RTT.

Keywords Rett syndrome . MeCP2 , Astrocytes , Microtubules , Tubastatin A , HDAC6

1. Introduction

Rett syndrome (RTT, MIM 3127750) is a rare X-linked neurodevelopmental disorder, characterized by ~ 6–18 months of normal development and subsequent cognitive regression. RTT individuals develop progressively lose acquired motor and language skills, stereotypic hand movements, and develop major respiratory problems, seizures, autistic-like behaviors, increased anxiety-like behaviors, and severe cognitive impairment (Bienvenu and Chelly, 2006; Ricceri et al., 2012). Pathogenic variants in the methyl CpG binding protein 2 gene (*MECP2*) cause > 95% of classical cases (Amir et al., 1999; Chahrour et al., 2007; Guy et al., 2011; Tillotson et al., 2019). Moreover, *MECP2* variants have been involved in a spectrum of neuropsychiatric phenotypes in both females and males (Biancardi et al., 2016; Schönewolf-Greulich et al., 2016; Curie et al., 2017; Skeikh et al., 2018). *MECP2* encodes for a multifunctional protein that binds to methylated DNA and to the NCoR1/2 corepressor complex, mainly acting as a global gene expression modulator, particularly in neurons but also in astrocytes (Bienvenu and Chelly, 2006; Guy et al., 2011; Tillotson et al., 2019). Although there is no cure for this devastating disorder, reactivation of Mecp2 in symptomatic Mecp2-deficient mice leads to phenotypic reversal (Guy et al., 2007). This finding, reinforced by the rescue of the behavioural phenotypes of mice overexpressing Mecp2 (Sztainberg et al., 2015), provides hope that RTT will be curable.

Earlier studies suggested the idea that RTT is caused exclusively from loss of Mecp2 function in neurons. Several studies, however, have shown that Mecp2 is clearly expressed in all glial cell types including astrocytes and oligodendrocytes (Ballas et al., 2009; Lioy et al., 2011; Okabe et al., 2012), and that glia, like neurons, are integral components of the neuropathology of RTT (Lioy et al., 2011; Kahanovitch et al., 2019; Cresto et al., 2019; Dong et al., 2020). Though much is known about microtubule organization and microtubule-based transport in neurons, the development and function of microtubules in glia are more enigmatic. However, several key papers implicated glial microtubule defects in neurological injury and disease (Weigel et al., 2021) and linked the loss of MECP2 in astrocytes to the appearance and progression of the RTT phenotype in a non-cell autonomous manner (Ehinger al., 2021).”

Several lines of mice carrying *Mecp2* mutations are now available. Shortly after the creation of *Mecp2*-null mice, a new line of mice expressing a truncated form of Mecp2 (Mecp2 ^{308}) was generated. This type of mutation is commonly found in classic RTT (Shahbazian et al., 2002). We previously analyzed microtubule (MT) dynamics in cortical neurons and astrocytes from *Mecp2* $^{308/y}$ mice (Nectoux et al., 2012). Our data revealed a dramatically increased microtubule growth rate in Mecp2-deficient astrocytes from newborn Mecp2-deficient mice compared to that of their control wild-type littermates (Nectoux et al., 2012), suggesting a dynamic balance impairment in favor of a destabilized state. This suggested the use of MT stabilizing molecules as an approach to compensate for Mecp2 loss-of-function (Brunden et al., 2011). We first tested this strategy with the MT-stabilizing drug paclitaxel (Taxol), on MeCP2-deficient fibroblasts (Nectoux et al., 2012). While microtubule dynamic impairment was indeed counteracted by the treatment, paclitaxel is not suitable for human neurodevelopmental disorders because of poor blood–brain barrier (BBB) permeability (Brunden et al., 2011). Another approach is then to use molecules that increase tubulin acetylation, post-translational modification frequently associated with microtubule stability (Hubbert et al., 2002; Matsuyama et al., 2002; Zhang et al., 2003). Acetylation of the ε-amino group of lysine-40 of α-tubulin is mediated by acetyltransferase, while deacetylation is mediated by histone deacetylase 6 (HDAC6). Increased levels of HDAC6 have been characterized in Mecp2-deficient tissues (Gold et al., 2015; Delépine et al., 2016). Tubastatin A, a tetrahydro-γ-carboline-capped selective HDAC6 inhibitor (HDAC6i), was rationally designed 10 years ago, and has become the best investigated HDAC6i to date. It shows efficacy in various neurological disease animal models, as HDAC6 plays a crucial regulatory role in axonal transport deficits, protein aggregation, as well as oxidative stress (Shen et al., 2020). Tubastatin A selectively inhibits HDAC6 with great specificity (Butler et al., 2010). It has been shown to stabilize microtubules against cold and nocodazole-induced depolymerization with a concomitant increase in HDAC6 binding to the microtubules in MCF-7 cells, demonstrating its ability to stabilize the microtubule network (Asthana et al., 2013). It was shown that Tubastatin A counteracted the microtubule defects observed in MeCP2-deficient fibroblasts from RTT patients, which could in turn lead to the restoration of molecular trafficking along the microtubules (Gold et al., 2015). Moreover, Tubastatin A can cross the BBB and was shown to correct neuronal defects and reverse certain phenotypic

abnormalities associated with aberrant microtubule-mediated transport of mitochondria in a mouse model of Charcot-Marie-Tooth disease (d'Ydewalle et al., 2011). Tubastatin A has also been shown to increase the anterograde and retrograde velocity of BDNF vesicles in cultured neurons from Mecp2 knockout mice, as well as to restore the activity-dependent release of BDNF to the release levels of wild-type neurons (Xu et al., 2014). Finally, HDAC6 inhibition reversed ciliogenesis defects in Mecp2-mutated cells with a concomitant amelioration of their typical neuronal dysfunction (Frasca et al., 2020). All these data suggest that microtubules instability and the associated deficits in intracellular trafficking contribute to the RTT phenotype, and that TBA has protective effects *in vitro* for a variety of cell types. However the effects of TBA treatment on astrocyte defecits in microtubule-associated vesicular transport have not been investigated yet, nor the efficacy of TBA treatment to rescue RTT-associated symptoms *in vivo*.

The main goal of this work was to generate preclinical findings in an effort to enhance the predictive value of our translational research. The effect of a Tubastatin A treatment on reversing early RTT-related abnormalities was therefore investigated in a *Mecp2* $^{308/y}$ mouse model. In this preclinical study, we identified in mice a safe and effective drug, that we hope could be used in future RTT patient clinical trials.

2. Results

2.1. The histone deacetylase 6 (HDAC6) inhibitor, Tubastatin A, corrects the vesicular mobility defect in Mecp2-deficient astrocytes

To determine if MT-dependent vesicle transport was affected by MT dynamics defect in *Mecp2* $^{308/y}$ astrocytes, we measured the fraction of highly directional versus highly non-directional mobile vesicles as described previously (Potokar et al., 2005). Lysosome vesicles are transported along MTs, therefore astrocyte cultures were incubated for 1h with Lysotracker® and Lysotracker-positive lysosome vesicles were tracked during 2 min movies with a picture acquisition every 2 sec. Vesicles were classified as mobile vesicles by the criteria of a track length over 1µm (Stenovec et al., 2011). Lysotracker-positive mobile vesicles displayed complex motion patterns composed of forward and backward movements

interrupted by periods of arrested mobility. We distinguished vesicles moving in a highly directional fashion from vesicles moving in a highly non-directional fashion by measuring the ratio of displacement, meaning the distance between the first and the last positions, over the total track length of each mobile vesicle. Vesicles with a displacement under 20% of the total track length were classified as highly non-directional (ND). We observed that *Mecp2* $^{308/y}$ astrocytes presented a decreased percentage of mobile vesicles (WT: n=19 cells, Mean ± SEM = 58.35 ± 3.046; *Mecp2* $^{308/y}$: n=23 cells, Mean ± SEM = 48.57 ± 2.796; p-value = 0.0237, unpaired t-test, Two-tailed), and, among those mobile vesicles, an increased percentage of vesicles moving in a highly non-directional fashion in comparison with WT astrocytes (WT: n=19 cells, Mean ± SEM = 45.34 ± 2.604; *Mecp2* $^{308/y}$: n=17 cells, Mean ± SEM = 55.59 ± 3.674; p-value = 0.0269, unpaired t-test, Two-tailed) (see Fig.1).

To determine whether Tubastatin A could stabilize microtubules and rescue the vesicle directionality of Mecp2-deficient astrocytes *in vitro*, mouse *Mecp2* $^{308/y}$ astrocytes were treated with 100 nM Tubastatin A for 24h before performing lysosome tracking (see Fig.1). *Mecp2* $^{308/y}$ astrocytes treated with Tubastatin A demonstrated an increased vesicle average speed (*Mecp2* $^{308/y}$ TBA: n=18 cells, Mean ± SEM = 0.09111 ± 0.0003782; *Mecp2* $^{308/y}$ vehicle: n=23 cells, Mean ± SEM = 0.07 ± 0.003719 ; p-value = 0.0003, unpaired t-test, Two-tailed) and track length (*Mecp2* $^{308/y}$ TBA: n=18 cells, Mean ± SEM = 1.874 ± 0.08297; *Mecp2* $^{308/y}$ vehicle: n=23 cells, Mean ± SEM = 1.462 ± 0.1028 ; p-value = 0.01028, unpaired t-test, Two-tailed), as well as an increased percentage of mobile vesicles (*Mecp2* $^{308/y}$ TBA: n=18 cells, Mean ± SEM = 65.87 ± 2.006; *Mecp2* $^{308/y}$ vehicle: n=23 cells, Mean ± SEM = 48.57 ± 2.796 ; p-value < 0.0001, unpaired t-test, Two-tailed) with a reduced percentage of vesicles moving in a highly non-directional fashion in comparison with *Mecp2* $^{308/y}$ astrocytes treated with vehicle (*Mecp2* $^{308/y}$ TBA: n=18 cells, Mean ± SEM = 40.32 ± 3.048; *Mecp2* $^{308/y}$ vehicle: n=17 cells, Mean ± SEM = 55.59 ± 3.674; p-value = 0.0029, unpaired t-test, Two-tailed). Thus, Tubastatin A is able to rescue the vesicle directionality of Mecp2-deficient astrocytes *in vitro*, reinforcing the idea that impairment of MT dynamics leads to vesicular trafficking alteration in RTT, and can be corrected by TBA.

2.2. Tubastatin A corrects some behavioral symptoms of *Mecp2* $^{308/y}$ male mice

Based on our *in vitro* data, we investigated the effects of chronic administration of Tubastatin A in a mouse model of Rett Syndrome. Five-weeks-old *Mecp2* $^{308/y}$ mice were treated with daily intraperitoneal injection of TBA at the dose of 25 mg/kg. A tailored battery of validated behavioral tests was carried out on a 12 weeks treatment schedule.

2.2.1. Open field test

In order to clarify the effects of tubastatin A treatment on general locomotor activity, *MeCP2* $^{308/y}$ mice and wildtype littermates were tested using an open field test. Overall locomotor activity and rears were comparable between genotypes and treatments [Genotype $F(1,33)\leq 0.35$, NS; Treatment $F(1,33)\leq 0.01$, NS; interaction Genotype*Treatment $F(1,33)\leq 0.61$, NS] (see Fig.2). Exploration of the center part of the arena was not affected by the genotype nor by the treatment, as reflected by the percentage of time spent in the central area[Genotype $F(1,33)=0.04$, NS; Treatment $F(1,33)=0.34$, NS; interaction Genotype*Treatment $F(1,33)=0.04$, NS] (see Fig.2). The tubastatin A treatment did not affect the general activity and anxiety-related behavior of wildtype and mutant mice in this test.

2.2.2. Water maze

To evaluate the potential effect of *Mecp2* $^{308/y}$ mutation and TBA treatment on spatial learning and memory, we used the hidden platform version of the Morris water maze to test the same mice at the age of 17 weeks (see Fig.3). This task requires mice to swim in a pool of water to find a hidden platform by using only extramaze cues. The latency and distance traveled to locate the hidden platform were not affected by the genotype nor by the treatment [Genotype $F(1,32)\leq 0.84$, NS; Treatment $F(1,32)\leq 0.25$, NS; interaction Genotype*Treatment $F(1,32)\leq 0.40$] , and all the four groups evolved similarly as testing progressed (see Fig. 3).

When the platform was removed from the pool during the probe trial, the preference for quadrants and the number of platform position crosses were also comparable across all genotypes and treatments [Preference: Genotype $F(1,32)=0.03$, NS, Treatment $F(1,32)=0.97$, NS; platform crosses Genotype $F(1,32)=1.18$, NS; Treatment $F(1,32)=0.73$, NS)] (Fig. 3). These

results suggest that neither *Mecp2* mutation nor Tubastatin A treatment affected spatial learning under our conditions.

When animals were required to locate a visible platform, the latency and distance traveled were also comparable across genotypes and across treatments [Genotype $F(1,32) \leq 0.14$, NS; Treatment $F(1,32) \leq 0.43$, NS; interaction Genotype*Treatment $F(1,32) \leq 1.30$], suggesting that visual and swimming abilities were not altered (see Fig. 1S).

2.2.3. Elevated plus maze

In the elevated plus maze, the percentage of entries and percentage of time spent in the open arms were not affected by the genotype nor by the treatment [Genotype $F(1,33) \leq 1.01$, NS; Treatment $F(1,33)) \leq 0.39$, NS] (see Fig. 4). The number of closed arm entries was also comparable across all groups [Genotype $F(1,33)=0.26$, NS; Treatment $F(1,33)=2.30$, NS] (see Fig. 4).

2.2.4. Marble burying

The percentage of marbles that were at least 2/3 covered by mice during the test session showed a significant effect of Genotype and Genotype*Treatment interaction [Genotype $F(1,33)=11.67$, $p<0.01$; Treatment $F(1,33)=3.59$, NS; Interaction $F(1,33)=14.94$, $p<0.001$]. *Mecp2* $^{308/y}$ mice treated with vehicle showed a significantly lower proportion of covered marbles compared to their WT counterparts ($p<0.001$; Student Newmann Keuls) (see Fig. 5), indicating a decrease in environment-directed exploratory behaviour in *Mecp2* $^{308/y}$ mutants, consistent with previous reports (Delépine et al., 2016; De Fillipis et al., 2015). Interestingly, Tubastatin A-treated *Mecp2* mutants showed a significantly larger proportion of covered marbles than vehicle-treated *Mecp2* mice ($p<0.001$, Student Newmann Keuls), indicating that Tubastatin A restored the impaired exploratory behaviour in *Mecp2* mutants (see Fig. 5).

2.3. Western blot and RT-PCR analysis

To evaluate the tubulin acetylation levels of brain tissues in *Mecp2* $^{308/Y}$ mutant mice and the molecular effects of tubastatin A *in vivo*, untreated and TBA-treated WT- and *Mecp2* $^{308/y}$ mice at 17 week-old were euthanized by cervical dislocation, and their brains collected within

the first 2min post-mortem. The hippocampus and amygdala, brain regions associated with anxiety, were microdissected.

HDAC6 deacetylase activity was estimated by Western Blot quantification of acetyl-tubulin levels. Consistent with our previous report (Delépine et al., 2016), Mecp2 deficiency decreased tubulin acetylation levels (see Fig. 6), suggesting a reduction in deacetylation activity of HDAC6 (p=0.09 hippocampus; p=0.0008 amygdala) (n=10; WT vehicle 1+/-0.058 vs *Mecp2* $^{308/y}$ KO vehicle 0.682+/-0.172, p=0.09 in hippocampus; n=16; WT vehicle 1+/-0.033 vs *Mecp2* $^{308/y}$ KO vehicle 0.710+/-0.097, p=0.0008 in amygdala). We also showed that tubastatin A treatment in *Mecp2* $^{308/y}$ mice restored the level of acetylated tubulin as well as the acetylated tubulin / total tubulin ratio in the hippocampus (n=10; *Mecp2* $^{308/y}$ KO vehicle 0.682+/-0.172 vs *Mecp2* $^{308/y}$ KO TBA 1.135+/- 0.069, p=0.0758), but did not do so significantly in the amygdala (n=16; *Mecp2* $^{308/y}$ KO vehicle 0.710+/-0.097 vs *Mecp2* $^{308/y}$ KO TBA 0.767+/-0.094, p=0.8957) (see Fig.6).

Moreover, it has been previously shown that at P55, levels of Hap1, a protein involved in Bdnf trafficking, were decreased in some brain regions (Roux et al., 2012). We did not observe any significant difference in Hap1 protein levels in 17-week *Mecp2* $^{308/y}$ mice in the tested brain regions (hippocampus and amygdala) (data not shown), although interestingly we observed a significant reduction of *Hap1* mRNA expression in the hippocampus (WT vehicle 1+/-0.134 vs *Mecp2* $^{308/y}$ KO vehicle 0.744+/-0.147, p=0.042) and a slight trend towards a decrease in expression in the amygdala (WT vehicle 1+/-0.137 vs *Mecp2* $^{308/y}$ KO vehicle 0.898+/-0.094, p=0.13) (see Fig.7). After drug treatment, *Hap1* mRNA levels increased slightly in the hippocampus, but not in the amygdala.

3. Discussion

Microtubules (MTs) are highly dynamic structures and the regulation of MT dynamics is crucial for cellular functions such as migration, division, polarity and differentiation. One growing hypothesis to explain the MT instability is that post-translational modifications of tubulin dynamically regulate MT functions. Among them, the acetylation of α-tubulin at lysine 40 is found on stable MTs in most cell type. Although the relationship between tubulin

acetylation and MT stability is not completely understood, acetylated-tubulin is often considered to be a marker for stable MTs. This post-translational modification has also been reported to play a positive role in motor-based trafficking (Palazzo et al., 2003; Reed et al., 2006; Dompierre et al., 2007). Two enzymes, HDAC6 and SIRT2, have been shown to deacetylate α-tubulin *in vitro* and *in vivo* (North et al., 2003).

Potokar and colleagues revealed the contribution of MTs to directional vesicle mobility in astrocytes (Potokar et al., 2013). Vesicles were characterized as highly directional when vesicle tracks displayed a straight line, and highly non-directional when vesicle tracks displayed a contorted line. In line with those studies, we previously showed that the percentage of highly non-directional vesicles was increased in *Mecp2* $^{308/y}$ astrocytes compared to wild-type astrocytes and could be rescue by a MT stabilizer analogue to taxol (Delépine et al., 2016). We also reported high levels of HDAC6 and low levels of tubulin acetylation in *Mecp2* $^{308/y}$ cultured astrocytes compared to that of wild-type (Delépine et al., 2016). In this study, we reported that *Mecp2* $^{308/y}$ astrocytes treated with HDAC6 inhibitor TBA presented a reduced percentage of vesicles moving in a highly non-directional fashion in comparison with *Mecp2* $^{308/y}$ astrocytes treated with vehicle. TBA is thus able to rescue the vesicle directionality of Mecp2-deficient astrocytes *in vitro*, reinforcing the idea that impairment of MT dynamics through increased deacetylation of α-tubulin, by increased levels of HDAC6, leads to vesicular trafficking alteration in RTT. A previous report has also shown that primary cilium defects associated with abnormal Sonic Hedgehog pathway have been observed in RTT neurons and fibroblasts and were rescued by HDAC6 inhibition (Frasca et al., 2020). Together, these results suggest that Mecp2 deficiency globally affects MT-dependent transport through HDAC6-dependent mechanisms. The effect of Mecp2 on microtubules may be direct by interaction with microtubules or indirect by altered expression on proteins involved in microtubule dynamics (Miyake K et al., 2007).

Considering our *in vitro* results, we conducted an *in vivo* study on the effect of Tubastatin A administered before the development of severe symptoms, including loss of locomotion and/or seizures, in *Mecp2* $^{308/y}$ mice. Several studies have evaluated the effects of different drug candidates in old mice when secondary brain dysfunctions were observed. Because RTT patients can only be diagnosed after the beginning of the regression period (9~18 months),

we started the treatment on early asymptomatic *Mecp2* $^{308/y}$ mice (one month-old i.e. 5 weeks-old) and continued for 12 weeks up to the end of behavioural testing. At 17 weeks of age, overall the motor activity, locomotor activity, and rears were comparable between genotypes and treatments in the open field, water-maze, and elevated maze assays. The tubastatin A treatment did not affect the general activity, learning, memory, or anxiety-related behavior of either WT or mutant mice. Because we chose to study early events in *Mecp2* $^{308/y}$ male mice, several behavioral tests did not reveal any genotype nor treatment effect. Further studies in other models with most severe phenotype will be needed to confirm our conclusions. However, in the marble burying test, the percentage of marbles at least 2/3 covered by the mice during the test session was significantly decreased for vehicle-treated *Mecp2* $^{308/y}$ mice as compared to vehicle-treated WT mice. It has been previously shown that in the Marble Burying test, *Mecp2* $^{308/y}$ mice displayed decreased digging and buried a lower number of marbles compared with WT littermates, indicating decreased environment-directed exploratory behavior (Delépine et al., 2016; Gyertyan et al., 1995). Interestingly, TBA-treated *Mecp2* $^{308/y}$ TBA mice showed a significantly increased percentage of 2/3 covered marbles as compared to vehicle-treated *Mecp2* $^{308/y}$ mice. Even though the marble burying behavior has been interpreted as a manifestation of stereotypic behavior and/or increased anxiety (Thomas et al., 2009), other authors suggested that the number of marbles buried simply provided an indirect measurement of exploratory behavior (i.e. digging) (Deacon et al., 2006). De Filippis and colleagues previously described that *Mecp2* $^{308/y}$ mice had a decreased marble burying behavior that might reflect an impairment of the environment-directed exploratory behavior (De Fillipis et al., 2010; De Fillipis et al., 2015). Consistent with these observations, the fact that an histone deacetylase HDAC6 inhibitor and epothilone D (Delépine et al., 2016), a microtubule-stabilizing agent, showed similar results on this test demonstrates that the early impairment of the environment-directed exploratory behavior in these Mecp2-deficient mice is due to abnormal stability of microtubules in the brain. The present findings demonstrate that the tubastatin treatment exerts beneficial effects on the performance of *Mecp2* $^{308/y}$ mice in the Marble burying behavior, and provide an early step in considering TBA in the strategy for RTT treatment. It is noteworthy that, except the marble burying test which provided strong proof of concept value on beneficial effect of TBA, *Mecp2* $^{308/y}$ mutants did not display any alteration in the

openfield, elevated plus maze or the water maze to evaluate the potency of TBA treatment. Further studies using other behavioral tests revealing stronger effects might provide additional insight into preclinical relevance of TBA in correcting RTT-like symptoms. For example, home cage monitoring might provide long-term measurement of general activity and stereotypic behavior without intervention of the experimenter; we found that *Mecp2* $^{308/y}$ displayed decreased ambulatory activity and local activity (which can be interpreted as stereotypic behavior), both restored with Epothilone D (data not published). The acoustic startle and PPI measuring sensorimotor gating altered in neuropsychiatric diseases was also altered in Mecp2 mutants (data not published). Otherwise, the light/Dark test (a well-established paradigm for the assessment of the anxiety-related profile), the burrowing test, or the digging behavior discrimination test might be used to extend the phenotypic profile of Mecp2 mutants and the potential of TBA to reverse efficiently such behavioral alterations (Pond et al. 2021).

We then interrogated the HDAC6-dependant molecular mechanisms of the deficits in microtubule stability, intracellular transport, and environment-directed exploratory behavior associated with Mecp2 deficiency. Because we showed early abnormal exploratory behavior, we examined the level of acetylated α-tubulin (K40), a major substrate of HDAC6, in brain structures involved in anxiety (amygdala) and exploratory behavior (hippocampus). We detected a reduction of acetyl-α-tubulin / tubulin ratio in the hippocampus of *Mecp2* $^{308/y}$ vehicle mice as compared to WT vehicle mice, although not statistically significant, and observed that it was significantly corrected by the TBA treatment. Further studies using a larger cohort would be needed to confirm our results. Based on the results presented here, we speculate that tubastatin-induced tubulin acetylation might account for the beneficial effects on microtubule dynamics and on the performance of *Mecp2* $^{308/y}$ mice. However, we can not exclude that other mechanisms, such as tubulin trimethylation or tyrosination, might have contributed to modification of microtubule dynamics.

Using the same brain structures, the amygdala and the hippocampus, we analyzed the expression of the *HAP1* gene, previously shown to be dysregulated in Mecp2 KO mice, and known to be involved in intracellular transport (Roux et al., 2012). Interestingly, we showed a significant decrease in *Hap1* mRNA expression in the hippocampus. HAP1 is a kinesin-1

adaptor involved in the trafficking of several neuronal transmembrane proteins (Twelvetrees et al., 2019). Previous data obtained using real-time quantitative PCR showed that *Hap1* mRNA levels were reduced at P55 in the medulla oblongata, in the pons, and in the rostral brain (Roux et al., 2012). Our results confirmed that *Hap1* mRNA expression was affected in certain brain regions, even in young *Mecp2* $^{308/y}$ mice before the appearance of the first major phenotypic manifestations. The decrease of *Hap1* expression could in turn affect the mRNA transport machinery (Ma et al., 2011) and could subsequently reduce neuronal transmembrane protein levels, protein trafficking, and neuronal exocytosis (Doppler et al., 2008).

In conclusion, the present report provides insights into the molecular bases of Rett syndrome and provide preliminary evidence that pharmacologically targeting microtubules in the brain using a HDAC6 inhibitor improves specific behavioral manifestation of Rett syndrome. This improvement may be the consequence of a better stabilization of the microtubule network and of a normalization of the expression of genes involved in neuronal mRNA trafficking (Miyake et al., 2007). Because we did not observe any early changes in the open field, Morris water maze, or elevated plus maze in our mouse model, further studies are needed to validate this hypothesis in other mouse models such as the full Mecp2 knock-out mice. Nonetheless, the present findings demonstrate that the tubastatin treatment exerts beneficial effects on the performance of *Mecp2* $^{308/y}$ mice in the Marble burying behavior, and provides an early step in considering TBA as a strategy for RTT treatment. Very recently, it has also been shown in a Rett Syndrome mouse model that early intensive training led to behavioural improvements, demonstrating the relevance of providing treatment before the onset of symptoms (Achilly et al., 2021).

4. Experimental procedure

4.1. Animals

The experimental subjects were 5 weeks of age hemizygous *Mecp2* $^{308/y}$ male mice and wild-type littermates (B6.129S-*Mecp2*<tm1Heto>/J, stock number: 005439; backcrossed to C57BL/6J mice for at least 12 generations from the Jackson Laboratories, USA) (Shahbazian et al., 2002; De Fillipis et al., 2010). All procedures were carried out in accordance with the

new European Communities Council Directive (2010/063 EU) and the implementing French decree of application n° 2013-118 01 and its supporting annexes entered into legislation 01 February 2013. All procedures were formally approved by local ethical committees from Paris Descartes University and the Com'Eth (n°17) for the laboratories in Illkirch.

4.2. Genotyping

Genotyping was performed by routine PCR technique according to The Jackson Laboratory protocols. The gender was determined using primers for the *Sry* gene on Y chromosome, which were 5'- CTC ATC GGA GGG CTA AAG TG -3' and 5'- AAG CTT TGC TGG TTT TTG GA -3'. Genotype was determined using primers for the *Mecp2* gene, which were 5'-AAC GGG GTA GAA AGC CTG-3', 5'-TGA TGG GGT CCT CAG AGC-3' and 5'-ATG CTC CAG ACT GCC TTG-3' for *Mecp2* $^{308/y}$ mice.

4.3. Cortical mouse astrocyte cultures

Primary astrocyte cultures were prepared from 1-day-old wild-type and *Mecp2* $^{308/y}$ mice, male cerebral cortex according to previously described methods (Gebicke-Haerter et al., 1989). Briefly, after removal of the meninges, forebrains were rinsed and gently dissociated by trituration following 30min incubation with trypsin 0.05% (Invitrogen, Cergy-Pontoise, France). Cells were collected by centrifugation at 300 x g for 3 min, resuspended in DMEM supplemented with 10% heat-inactivated FBS, plated in micro-dishes designed for live imaging (µ-Dish 35 mm; Ibidi, München, Germany) and incubated at 37°C in a humidified atmosphere of 95% air, 5% CO_2. Purity of the cell population, as determined by glial fibrillary acidic protein (GFAP) immunohistochemical staining, was > 99%. Each experiment was performed with astrocyte primary cultures from littermate newborn pups and each litter contained at least two *Mecp2* $^{308/y}$ and two wild-type pups.

4.4. Live cell tracking of lysosome vesicles

4.4.1. Fluorescent Staining and Confocal Microscopy

Acidic vesicles in two weeks *in vitro* confluent mouse astrocyte culture were loaded with 200 nM Lysotracker Red DND-99 (Invitrogen, Cergy Pontoise, France) in culture medium at

37 °C for 1h. Prior to imaging, cells were transferred to imaging medium. Cells were allowed to adapt to the new medium in ambient air for at least 30 min at 37°C. Image acquisition and image analysis were performed on the Cochin Imaging Facility. Live stained cells were imaged with an inverted confocal microscope (Zeiss Axiovert 200M) using oil immersion objective 63×/NA 1.4. Time-lapse confocal images were acquired every 2 s for 2min. Stacks were built using Meta Morph v7.5 (Molecular Devices, Silicon Valley, CA, USA) and analyzed using the IMARIS software (Bitplane, South Windsor, USA). About 100-200 vesicles were tracked in each cell. Independent experiments were repeated at least three times, a total of 17-19 cells were analyzed for each group.

4.4.2.Vesicle tracking and data analysis

Vesicle mobility was analyzed by IMARIS software (Bitplane, South Windsor, USA) to obtain several mobility parameters (Potokar et al. , 2005). Briefly, a 2D Gaussian curve was fitted on the selected vesicles in each image within the time series, and the *x*- and *y*-coordinates of the peaks of the curves were connected to acquire tracks of vesicle mobility (trajectories). The current time (time from the beginning of single vesicle tracking), average speed, displacement length (distance between the first and last spot position), and track length (TL, the total length of the analyzed vesicle pathway) were determined and the ratio of the displacement, meaning the distance between the first and the last spot position, over the total track length of each mobile vesicle were measured to analyze vesicle directionality.

4.5. Tubastatine A or vehicle treatment of *Mecp2* $^{308/y}$ and wild-type mice

Tubastatin A was dissolved in vehicle solution, i.e., sodium chloride 0.9%. Groups of 5-week-old male *Mecp2* $^{308/y}$ mice (n=18) or wild-type littermates (n=19) were administered daily intraperitoneal injections of 25 mg/kg tubastatin A (Selleckchem, S8049, with IC50 of 15nM in a cell-free assay), or vehicle, for a total of 12 consecutive weeks (3 months). Experiments were performed according to guidelines concerning randomization and blinding. Treatment continued throughout behavioral testing. We choose to focus on male *Mecp2* $^{308/y}$ mice because of the unpredictability of heterozygous females phenotype deriving from the X-chromosome inactivation phenomena and because male mice develop neurodevelopmental pathology more consistently than females. Indeed, hemizygote male mice allow eliminating the confounding effects of a variable phenotype while investigating the role of *Mecp2* gene

mutations on the development of RTT-like symptoms. Animals were monitored for signs of abnormal behavior or distress, and were weighed weekly. After 12 weeks of dosing, the mice were submitted to specialized behavioural testing as described below.

4.6. Behavioral Analyses

Mice were submitted to tests allowing evaluation of general health and sensory-motor abilities, anxiety-related behavior, learning and memory, and social behavior.

4.6.1. Gross neurological examination

The general health and basic sensory motor functions were evaluated using a modified SHIRPA protocol (EMPRESS, eumorphia.org). This analysis, which is adapted from the SHIRPA protocol, provides an overview of physical appearance, and body weight, as well as body temperature, neurological reflexes and sensory abilities (Hatcher et al., 2001).

4.6.2. Emotional & social behavior

Elevated plus maze: The apparatus used is completely automated and made of PVC (Imetronic, Pessac, France). It consists of two open arms (30 X 5 cm) opposite one to the other and crossed by two enclosed arms (30 x 5 x 15 cm). The apparatus is equipped with infrared captors allowing the detection of the mouse in the enclosed arms and different areas of the open arms. Mice were tested for 5 min during which the number of entries into and time spent in the open arms were measured and used as an index of anxiety. Closed arm entries and total arm entries were used as measures of general motor activity.

The open field test: Mice were tested in automated open fields (Panlab, Barcelona, Spain), each virtually divided into central and peripheral regions. The open fields were placed in a room homogeneously illuminated at 150 Lux. Each mouse was placed in the periphery of the open field and allowed to explore freely the apparatus for 30 min, with the experimenter out of the animal's sight. The distance traveled, the number of rears, and time spent in the central and peripheral regions were recorded over the test session. The number of entries and the percent time spent in center area are used as index of emotionality/anxiety.

Marble burying test: Twenty-four small marbles arranged in 5x4 rows in clean Plexiglas cages containing fresh bedding that was around 4 cm deep. Mice were introduced individually into this test arena and allowed to remain for 10 min under dim light and white-noise conditions. At the end of 10 min, the mouse was removed and the number of buried marbles was counted. A threshold of 2/3 coverage was used to determine whether the marbles were buried.

4.6.3. Learning and memory

Water maze: The water maze consisted of a white circular tank (1.50 m diameter) filled with opaque water. Pool temperature was adjusted to 21+1°C. For the hidden platform task, the escape platform (10 cm diameter) was positioned 1cm below water level in the center of one of the pool quadrants. For the cued task, platform position was signaled by the addition of a small flag. The walls surrounding the water maze were hung with posters and flags, which served as visual cues and are visible during all stages of training and testing. Movement of mice within the pool was tracked and analyzed with a computerized tracking system. Animals were first trained in the hidden platform protocol (spatial learning). Mice were required to locate a submerged hidden platform by using only extra-maze cues. Each mouse received 5 blocks of 4 training trials over five consecutive days in which they were placed in the pool at one of four randomized start positions (NE, SE, SW, NW), and allowed to locate the hidden platform. Trials lasted for a maximum of 120s and were separated by 15-20 min intervals. If a mouse failed to find the platform within this period, it is guided to its position by the experimenter. Spatial learning performance was assessed during a probe trial 1h after training, for which the target platform was removed from the pool. Mice were then tested for cued training (visible platform), in which they were placed in the pool facing the edge at one of four start positions (NE, SE, SW, NW), and required to locate a flagged platform whose position varies across trials. Each mouse received 4 trials per day for 2 consecutive days. Trials lasted for a maximum of 120s and were separated by 15-20 min intervals. The latency, distance and the average speed were used to evaluate performance during training trial. For the probe trial, the percentage of time in each quadrant and the number of platform crosses were used as index of spatial learning performance.

4.7. Immunoassay

To investigate the effects of tubastatin A in *Mecp2* $^{308/Y}$ mutant mice on tubulin acetylation, untreated and TBA-treated WT- and Mecp2 $^{308/y}$ male mice at 17 week-old were anesthetized by intraperitoneal injection (100 µl) of Ketamine (150mg/Kg)- Xylasin (10 mg/Kg) and then intracardially perfused with 4% paraformaldehyde (PFA) in 0.1 M PBS, pH 7.4 and post-fixed over-night in 4% PFA at 4°C. Their brains were collected out, and after cryoprotective immersion in 30% sucrose, each brain sample was kept at −80 °C. The hippocampus and amygdala were microdissected using a punching needle. Briefly, brain area dissection was performed on microtome HM450 (MM France, Brignais, France) brain sections with the help of a binocular magnifier, following their stereotaxic coordinates (Amygdala, bregma -1.34 _ -2.18 and hippocampus bregma -1.94 _ -2.46). Proteins were extracted and isolated in a lysis Laemmli buffer by incubation 20 minutes at 95°C. After denaturation, the protein samples were separated by a 4–20% Mini-PROTEAN® TGX Stain-Free™ Protein Gel (Bio-Rad, Hercules, California, United States) electrophoresis and then transferred onto a NC45 nitrocellulose membrane (SERVA electrophoresis GmbH, Heidelberg, Germany). The membrane was blocked with blocking buffer (TBS-Tween 20 0.05%/ 5% fat milk solution) for one hour at room temperature. Primary antibodies for HAP1 (BD 611302, 1/250), alpha-tubulin (DM1A, 1/1000) and acetylated tubulin (clone 6 11-B-1, , 1/4000) were diluted and incubated overnight at 4°C. The membrane was incubated using appropriate horseradish peroxidase (HRP)-conjugated secondary antibodies (anti-mouse or anti-rabbit) (Santa Cruz Biotechnology, Dallas, Texas, United States). The membranes were washed, incubated and developed with the enhanced chemiluminescence method (Clarity or Clarity Max Enhanced chemiluminescence (ECL) Substrate (Bio-Rad)) on a Chemidoc system (Bio-Rad). We also probed membranes for GAPDH (antibody anti-Gapdh Ambion, dilution 1/3000) for loading normalization. Quantification of protein levels was measured by the chemiluminescence intensity. Quantitative analyses of signal intensity were performed using ImageLab6.0 software (Bio-Rad). Specifically, for tubulin/acetylated tubulin, primary antibodies were stripped 15 minutes at 70°C in Restore™ PLUS Western Blot Stripping Buffer (Thermo Fisher Scientific) with 100mM DTT before the second protein revelation.

4.8. Quantitative RT-PCR

Tissues were incubated 1 hour at 56°C in 190µL of buffer (200 mM Tris–HCl,200mM NaCl,1.5mM MgCl2,2%SDS,pH8) with 10µL proteinase K (10mg/mL). Total RNA Extraction was completed by RNA clean up procedure of RNeasy kit (Qiagen, Hilden, Germany) and by RW1 washing procedure. RNA quality was evaluated on a 1% agarose gel. Total RNA from brain structures (amygdala, hippocampus) were converted to cDNA with Maxima First Strand cDNA synthesis Kit (ThermoScientific, Rochester, USA) with a dsDNase step (Thermo-Fisher Scientific Waltham, Massachusetts, United States), for quantitative real-time PCR with LightCycler® 480 SYBR Green I Master reagent (Roche Molecular Diagnostics) as detection agent with the LightCycler480 detection system (Roche Molecular Diagnostics, Pleasanton, California, United States). Primer sequences (specific for *Hap1* gene) are available on request. After PCR amplification, a dissociation protocol was performed to determine the melting curve of the PCR product. Normalization factor was based on housekeeping gene *Gapdh* and *Ppia.*

4.9. Data analysis

Behavioural data were analyzed using two or three factor ANOVA with repeated measures (Genotype, Treatment, time). Student Newmann Keuls post-hoc was used to compare performance between 2 groups. P-value <0.05 was considered statistically significant. Quantitative data from live cell tracking of lysosome vesicles were analyzed by Student t-test. For all other comparisons involving multiple variables, two-way ANOVA was performed followed by post hoc test for multiple comparisons using $p<0.05$ for significance. For all molecular experiments, 10-16 animals per experiment were used, with the number per group stated in each figure legend. Mean and SEM are indicated in the results section. All statistical analyses were performed using GraphPad Prism 5 (GraphPad Software, La Jolla, CA, USA).

Author funding

This work was supported by Fondation Jerome Lejeune (project#1557). This work was supported by the French state funds through the “Agence Nationale de la Recherche” under the frame programme Investissements d’Avenir labelled (ANR-10-IDEX-0002-02, ANR-10-LABX-0030-INRT, ANR-10-INBS- 07 PHENOMIN to Y.H.) and the National Institute of Health (U01 AG029213-01A2).

Declaration of interest

The authors declare that they have no competing interest. All authors declare no potential conflicts of interest.

Availability of data and material

The data generated during the current study are available from the corresponding author on reasonable request.

Author's contributions

Thierry Bienvenu developed the project. Thierry Bienvenu, Nicolas Lebrun, Hamid Meziane , Juliette Nectoux and Yann Herault designed the study and analysed and interpreted the data. Nicolas Lebrun, Chloé Delépine, Mohamed Selloum and Hamid Meziane performed the experiments. Nicolas Lebrun, Chloé Delépine, Hamid Meziane and Juliette Nectoux, performed and analysed the data. All authors approved the final version of the manuscript.

Ethics approval

All procedures were carried out in accordance with the new European Communities Council Directive (2010/063 EU) and the implementing French decree of application n° 2013-118 01 and its supporting annexes entered into legislation 01 February 2013. All procedures were formally approved by local ethical committees from Paris Descartes University and the Com'Eth (n°17) for the laboratories in Illkirch.

References

Achilly, N.P., Wang, W., Zoghbi, H.Y., 2021. Presymptomatic training mitigates functional deficits in a mouse model of Rett syndrome. Nature. Mar 24. doi: 10.1038/s41586-021-03369-7. Epub ahead of print. PMID: 33762729.

Amir, R.E., Van den Veyver, I.B., Wan, M., Tran, C.Q., Francke, U., Zoghb,i H.Y., 1999. Rett syndrome is caused by mutations in X-linked MECP2, encoding methyl-CpG-binding protein 2. Nat. Genet. 23, 185–188

Arystarkhova, E., Bouley, R., Liu, Y.B., Sweadner, K.J. 2017. Impaired AQP2 trafficking in Fxyd1 knockout mice: A role for FXYD1 in regulated vesicular transport. PLoS One. 12(11), e0188006. doi: 10.1371/journal.pone.0188006.

Asthana, J., Kapoor, S., Mohan, R., Panda, D., 2013. Inhibition of HDAC6 deacetylase activity increases its binding with microtubules and suppresses microtubule dynamic instability in MCF-7 cells. J. Biol. Chem. 288(31), 22516-22526.

Ballas, N., Lioy, D.T., Grunseich, C., Mandel, G., 2009. Non-cell autonomous influence of MeCP2-deficient glia on neuronal dendritic morphology. Nat. Neurosci. 12(3),311-317.

Bianciardi, L., Fichera, M., Failla, P., Di Marco, C., Grozeva, D., Mencarelli, M.A., Spiga, O., Mari, F., Meloni, I., Raymond, L., Renieri, A., Romano, C., Ariani, F., 2016. MECP2 missense mutations outside the canonical MBD and TRD domains in males with intellectual disability. J. Hum. Genet. 61, 95-101.

Bienvenu, T., Chelly, J. (2006). Molecular genetics of Rett syndrome: when DNA methylation goes unrecognized. Nature reviews. 7(6), 415-426.

Bhave, S.A., Uht, R.M., 2017. CpG methylation and the methyl CpG binding protein 2 (MeCP2) are required for restraining corticotropin releasing hormone (CRH) gene expression. Mol. Cell. Endocrinol. 454, 158-164. doi:10.1016/j.mce.2017.06.024.

Brunden, K.R., Yao, Y., Potuzak, J.S., Ferrer, N.I., Ballatore, C., James, M.J., Hogan, A.M., Trojanowski, J.Q., Smith, A.B. 3rd, Lee, V.M., 2011. The characterization ofmicrotubule-

stabilizing drugs as possible therapeutic agents for Alzheimer'sdisease and related tauopathies. Pharmacol. Res. 63(4), 341-351.

Butler, K.V., Kalin, J., Brochier, C., Vistoli, G., Langley, B., Kozikowski, A.P., 2010. Rational design and simple chemistry yield a superior, neuroprotective HDAC6 inhibitor, tubastatin A. J. Am. Chem. Soc. 132(31), 10842-10846. doi: 10.1021/ja102758v.

Chahrour, M., Zoghbi, H.Y., 2007. The story of Rett syndrome: from clinic to neurobiology. Neuron. 56, 422–437.

Cresto, N., Pillet, L.E., Billuart, P., Rouach, N., 2019. Do Astrocytes Play a Role in Intellectual Disabilities? Trends Neurosci. 42(8), 518-527. doi: 10.1016/j.tins.2019.05.011.

Curie, A., Lesca, G., Bussy, G., Manificat, S., Arnaud, V., Gonzalez, S., Revol, O., Calender, A., Gérard, D., des Portes, V., 2017. Asperger syndrome and early-onset schizophrenia associated with a novel MECP2 deleterious missense variant. Psychiatr. Genet. 27, 105-109. doi: 10.1097/YPG.0000000000000165. PMID: 28230711.

d'Ydewalle, C., Krishnan, J., Chiheb, D.M., Van Damme, P., Irobi, J., Kozikowski, A.P., Vanden Berghe, P., Timmerman, V., Robberecht, W., Van Den Bosch, L., 2011. HDAC6 inhibitors reverse axonal loss in a mouse model of mutant HSPB1-induced Charcot-Marie-Tooth disease. Nat. Med. 17(8),968-974. doi: 10.1038/nm.2396.

Deacon, R.M., 2006. Digging and marble burying in mice: simple methods for in vivo identification of biological impacts. Nat. Protoc. 1(1),122-124. doi: 10.1038/nprot.2006.20.

Delépine, C., Meziane, H., Nectoux, J., Opitz, M., Smith, A.B., Ballatore, C., Saillour, Y., Bennaceur-Griscelli, A., Chang, Q., Williams, E.C., Dahan, M., Duboin, A., Billuart, P., Herault, Y., Bienvenu, T., 2016. Altered microtubule dynamics and vesicular transport in mouse and human MeCP2-deficient astrocytes. Hum. Mol. Genet. 25(1),146-157.

De Filippis, B., Ricceri, L., Laviola, G., 2010. Early postnatal behavioral changes in the Mecp2-308 truncation mouse model of Rett syndrome.Genes Brain Behav. 9, 213–223.

De Filippis, B., Valenti, D., Chiodi, V., Ferrante, A., de Bari, L., Fiorentini, C., Domenici, M.R., Ricceri, L., Vacca, R.A., Fabbri, A., Laviola, G. (2015) Modulation of Rho GTPases rescues brain

mitochondrial dysfunction, cognitive deficits and aberrant synaptic plasticity in female mice modeling Rett syndrome. Eur. Neuropsychopharmacol. 25(6), 889-901. doi: 10.1016/j.euroneuro.2015.03.012.

Dompierre, J.P., Godin, J.D., Charrin, B.C., Cordelières, F.P., King, S.J., Humbert, S., Saudou, F., 2007. Histone deacetylase 6 inhibition compensates for the transport deficit in Huntington's disease by increasing tubulin acetylation. J. Neurosci. 27(13),3571-3583. doi: 10.1523/JNEUROSCI.0037-07.2007.

Dong, H.W., Erickson, K., Lee, J.R., Merritt, J., Fu, C., Neul, J.L., 2020. Detection of neurophysiological features in female R255X MeCP2 mutation mice. Neurobiol. Dis. 145,105083. doi: 10.1016/j.nbd.2020.105083.

Doppler, E., Rockenstein, E., Ubhi, K., Inglis, C., Mante, M., Adame, A., Crews, L., Hitzl, M., Moessler, H., Masliah, E., 2008. Neurotrophic effects of Cerebrolysin in the Mecp2(308/Y) transgenic model of Rett syndrome. Acta Neuropathol. 116(4), 425-437. doi: 10.1007/s00401-008-0407-x.

Ehinger, Y., Matagne, V., Cunin, V., Borloz, E., Seve, M., Bourgoin-Voillard, S., Borges-Correia, A., Villard, L., Roux, J.C., 2021. Analysis of Astroglial Secretomic Profile in the Mecp2-Deficient Male Mouse Model of Rett Syndrome. Int. J. Mol. Sci. 2021 22(9),4316. doi: 10.3390/ijms22094316. PMID: 33919253; PMCID: PMC8122273.

Frasca, A., Spiombi, E., Palmieri, M., Albizzati, E., Valente, M.M., Bergo, A., Leva, B., Kilstrup-Nielsen, C., Bianchi, F., Di Carlo, V., Di Cunto, F., Landsberger, N., 2020. MECP2 mutations affect ciliogenesis: a novel perspective for Rett syndrome and related disorders. EMBO Mol. Med. 12(6), e10270. doi: 10.15252/emmm.201910270.

Gebicke-Haerter, P.J., Bauer, J., Schobert, A., Northoff, H., 1989. Lipopolysaccharide-free conditions in primary astrocyte cultures allow growth and isolation of microglial cells. J. Neurosci. 9(1), 183-194. doi: 10.1523/JNEUROSCI.09-01-00183.1989.

Gold, W.A., Lacina, T.A., Cantrill, L.C., Christodoulou, J. (2015). MeCP2 deficiency is associated with reduced levels of tubulin acetylation and can be restored using HDAC6 inhibitors. J. Mol. Med. (Berl) 93(1),63-72.

Guy, J., Gan, J., Selfridge, J., Cobb, S., Bird, A., 2007. Reversal of neurological defects in a mouse model of Rett syndrome. Science. 315(5815),1143-1147. doi: 10.1126/science.1138389.

Guy, J., Cheval, H., Selfridge, J., Bird, A. (2011). The role of MeCP2 in the brain.Annu Rev Cell Dev Biol 27: 631–652.

Gyertyán, I., 1995. Analysis of the marble burying response: marbles serve to measure digging rather than evoke burying. Behav. Pharmacol. 6(1),24-31. PMID:11224308.

Hatcher, J.P., Jones, D.N., Rogers, D.C., Hatcher, P.D., Reavill, C., Hagan, J.J., Hunter, A.J., 2001. Development of SHIRPA to characterise the phenotype of gene-targeted mice. Behav. Brain Res. 125(1-2),43-47. doi: 10.1016/s0166-4328(01)00275-3.

Hubbert, C., Guardiola, A., Shao, R., Kawaguchi, Y., Ito, A., Nixon, A., Yoshida, M., Wang, X.F., Yao, T.P., 2002. HDAC6 is a microtubule-associated deacetylase. Nature 417(6887),455-458. doi: 10.1038/417455a. PMID: 12024216.

Kahanovitch, U., Patterson, K.C., Hernandez, R., Olsen, M.L., 2019. Glial Dysfunction in MeCP2 Deficiency Models: Implications for Rett Syndrome. Int. J. Mol. Sci. 20(15),3813. doi: 10.3390/ijms20153813. PMID: 31387202; PMCID: PMC6696322.

Lioy, D.T., Garg, S.K., Monaghan, C.E., Raber, J., Foust, K.D., Kaspar, B.K., Hirrlinger, P.G., Kirchhoff, F., Bissonnette, J.M., Ballas, N., Mandel, G., 2011. A role for glia in the progression of Rett's syndrome. Nature. 475(7357),497-500.

Ma, B., Savas, J.N., Yu, M.S., Culver, B.P., Chao, M.V., Tanese, N., 2011. Huntingtin mediates dendritic transport of β-actin mRNA in rat neurons. Sci. Rep. 1,140. doi: 10.1038/srep00140.

Matsuyama, A., Shimazu, T., Sumida, Y., Saito, A., Yoshimatsu, Y., Seigneurin-Berny, D., Osada, H., Komatsu, Y., Nishino, N., Khochbin, S., Horinouchi, S., Yoshida, M., 2002. In vivo destabilization of dynamic microtubules by HDAC6-mediated deacetylation. EMBO J. 21(24),6820-6831. doi: 10.1093/emboj/cdf682.

Miao, C.G., Yang, Y.Y., He, X., Li, J., 2013. New advances of DNA methylation and histone modifications in rheumatoid arthritis, with special emphasis on MeCP2. Cell. Signal. 25(4),875-882. doi: 10.1016/j.cellsig.2012.12.017.

Miyake, K., Nagai, K., 2007. Phosphorylation of methyl-CpG binding protein 2 (MeCP2) regulates the intracellular localization during neuronal cell differentiation. Neurochem. Int. 50(1),264-70. doi: 10.1016/j.neuint.2006.08.018. Epub 2006 Oct 18. PMID: 17052801.

Nectoux, J., Florian, C., Delepine, C., Bahi-Buisson, N., Khelfaoui, M., Reibel, S., Chelly, J., Bienvenu, T., 2012. Altered microtubule dynamics in Mecp2-deficient astrocytes. J. Neurosci. Res. 90(5),990-998.

North, B.J., Marshall, B.L., Borra, M.T., Denu, J.M., Verdin, E., 2003. The human Sir2 ortholog, SIRT2, is an NAD+-dependent tubulin deacetylase. Mol. Cell. 11,437-444.

Okabe, Y., Takahashi, T., Mitsumasu, C., Kosai, K., Tanaka, E., Matsuishi, T., 2012. Alterations of gene expression and glutamate clearance in astrocytes derived from an MeCP2-null mouse model of Rett syndrome. PLoS One. 7(4),e35354.

Palazzo, A., Ackerman, B., Gundersen, G.G., 2003. Cell biology: Tubulin acetylation and cell motility. Nature. 421(6920),230. doi: 10.1038/421230a.

Philippe, T.J., Vahid-Ansari, F., Donaldson, Z.R., Le François, B., Zahrai, A., Turcotte-Cardin, V., Daigle, M., James, J., Hen, R., Merali, Z., Albert, P.R., 2018. Loss of MeCP2 in adult 5-HT neurons induces 5-HT1A autoreceptors, with opposite sex-dependent anxiety and depression phenotypes Sci. Rep. 8(1),5788. doi: 10.1038/s41598-018-24167-8.

Pond, H.L., Heller, A.T., Gural, B.M., McKissick, O.P., Wilkinson, M.K., Manzini, M.C., 2021. Digging behavior discrimination test to probe burrowing and exploratory digging in male and female mice. J Neurosci. Res. May 28. doi: 10.1002/jnr.24857. Epub ahead of print. PMID: 34048600.

Potokar, M., Kreft, M., Pangrsic, T., Zorec, R., 2005. Vesicle mobility studied in cultured astrocytes. Biochem. Biophys. Res. Commun. 329(2),678-683.

Potokar, M., Vardjan, N., Stenovec, M., Gabrijel, M., Trkov, S., Jorgačevski, J., Kreft, M., Zorec, R., 2013. Astrocytic vesicle mobility in health and disease. Int. J. Mol. Sci. 14(6),11238-11258. doi: 10.3390/ijms140611238.

Reed, N.A., Cai, D., Blasius, T.L., Jih, G.T., Meyhofer, E., Gaertig, J., Verhey, K.J., 2006. Microtubule acetylation promotes kinesin-1 binding and transport. Curr. Biol. 16(21):2166-2172. doi: 10.1016/j.cub.2006.09.014.

Ricceri, L., De Filippis, B., Laviola, G., 2012. Rett syndrome treatment in mouse models: searching for effective targets and strategies. Neuropharmacology. 68:,106–115

Roux, J.C., Zala, D., Panayotis, N., Borges-Correia, A., Saudou, F., Villard, L., 2012. Modification of Mecp2 dosage alters axonal transport through the Huntingtin/Hap1 pathway. Neurobiol. Dis. 45(2),786-795. doi: 10.1016/j.nbd.2011.11.002.

Sheikh, T.I., Harripaul, R., Ayub, M., Vincent, J.B., 2018. MeCP2 AT-Hook1 mutations in patients with intellectual disability and/or schizophrenia disrupt DNA binding and chromatin compaction in vitro. Hum. Mutat. 39(5),717-728. doi: 10.1002/humu.23409. Epub 2018 Mar 8. PMID: 29431277.

Schönewolf-Greulich, B., Tejada, M.I., Stephens, K., Hadzsiev, K., Gauthier, J., Brøndum-Nielsen, K., Pfundt, R., Ravn, K., Maortua, H., Gener, B., Martínez-Bouzas, C., Piton, A., Rouleau, G., Clayton-Smith, J., Kleefstra, T., Bisgaard, A.M., Tümer, Z., 2016. The MECP2 variant c.925C>T (p.Arg309Trp) causes intellectual disability in both males and females without classic features of Rett syndrome. Clin. Genet. 89(6),733-738. doi: 10.1111/cge.12769. Epub 2016 Apr 8. PMID: 26936630.

Shahbazian, M., Young, J., Yuva-Paylor, L., Spencer, C., Antalffy, B., Noebels, J., Armstrong, D., Paylor, R., Zoghbi, H. (2002). Mice with truncated MeCP2 recapitulate many Rett syndrome features and display hyperacetylation of histone H3. Neuron. 35(2),243-254. doi: 10.1016/s0896-6273(02)00768-7. PMID: 12160743.

Shen, S., Svoboda, M., Zhang, G., Cavasin, M.A., Motlova, L., McKinsey, T.A., Eubanks, J.H., Bařinka, C., Kozikowski, A.P., 2020. Structural and in Vivo Characterization of Tubastatin A, a

Widely Used Histone Deacetylase 6 Inhibitor. ACS Med. Chem. Lett. 11(5),706-712. doi: 10.1021/acsmedchemlett.9b00560.

Sztainberg, Y., Chen, H.M., Swann, J.W., Hao, S., Tang, B., Wu, Z., Tang, J., Wan, Y.W., Liu, Z., Rigo, F., Zoghbi, H.Y., (2015) Reversal of phenotypes in MECP2 duplication mice using genetic rescue or antisense oligonucleotides. Nature. 528(7580),123-126. doi: 10.1038/nature16159.

Stenovec, M., Milošević, M., Petrušić, V., Potokar, M., Stević, Z., Prebil, M., Kreft, M., Trkov, S., Andjus, P.R., Zorec, R., (2011). Amyotrophic lateral sclerosis immunoglobulins G enhance the mobility of Lysotracker-labelled vesicles in cultured rat astrocytes. Acta Physiol.(Oxf). 203(4),457-471. doi: 10.1111/j.1748-1716.2011.02337.x.

Tavares, M.T., Kozikowski, A.P., Shen, S., (2021). Mercaptoacetamide: A promising zinc-binding group for the discovery of selective histone deacetylase 6 inhibitors. Eur. J. Med. Chem. 209,112887. doi: 10.1016/j.ejmech.2020.112887.

Thomas, A., Burant, A., Bui, N., Graham, D., Yuva-Paylor, L.A., Paylor, R., 2009. Marble burying reflects a repetitive and perseverative behavior more than novelty-induced anxiety. Psychopharmacology (Berl). 204(2),361-373. doi: 10.1007/s00213-009-1466-y.

Tillotson, R., Bird A., 2019. The Molecular Basis of MeCP2 Function in the Brain. J. Mol. Biol. 17:S0022-2836(19), 30595-30599. doi: 10.1016/j.jmb.2019.10.004.

Twelvetrees, A.E., Lesept, F., Holzbaur, E.L.F., Kittler, J.T., 2019. The adaptor proteins HAP1a and GRIP1 collaborate to activate the kinesin-1 isoform KIF5C. J. Cell. Sci. 132(24), jcs215822. doi: 10.1242/jcs.215822.

Weigel, M., Wang, L., Fu, M.M.,2021. Microtubule organization and dynamics in oligodendrocytes, astrocytes, and microglia. Dev. Neurobiol. 81(3),310-320.

Xu, X., Kozikowski, A.P., Pozzo-Miller, L., 2014. A selective histone deacetylase-6 inhibitor improves BDNF trafficking in hippocampal neurons from Mecp2 knockout mice: implications for Rett syndrome. Front. Cell. Neurosci. 7(8),68.

Yamanishi, K., Hashimoto, T., Miyauchi, M., Mukai, K., Ikubo, K., Uwa, N., Watanabe, Y., Ikawa, T., Okuzaki, D., Okamura, H., Yamanishi, H., Matsunaga, H., 2020. Analysis of genes

linked to depressive-like behaviors in interleukin-18-deficient mice: Gene expression profiles in the brain. Biomed. Rep. 12(1),3-10. doi: 10.3892/br.2019.1259.

Zhang, Y., Li, N., Caron, C., Matthias, G., Hess, D., Khochbin, S., Matthias, P., 2003. HDAC-6 interacts with and deacetylates tubulin and microtubules in vivo. EMBO J. 22(5),1168-1179. doi: 10.1093/emboj/cdg115.

Legends to Figures:

Fig. 1 Effect of Tubastatin (TBA) treatment on lysotracker-labelled vesicle mobility and directionality in Mecp2-deficient astrocytes. Cells were incubated 1h with 200nM LysoTrackerR and tubastatin A or vehicle before timelapse imaging. For each vesicle, speed, displacement length (DL) and total track length (TL) were measured by Imaris Software (Bitplane). A vesicle was considered mobile when its total track length was > 1µm and non-directional when its DL/TL ratio was <20%. We tracked 100-200 vesicles per cell. Bars represent the mean speed, track length, proportion of mobile vesicles, and proportion of non-directional mobile vesicles by cell +/- SEM.* indicates a p-value for Student test under 0.05, ** a p value under 0.01, *** a p value under 0.005, **** a p value under 0.001 and NS a p-value over 0.05. Non-directional fashion is characterized by a TDL (distance between last spot's position and first spot's position) / TL (total length of displacement) ratio lower than 20%.

Fig. 2 Behavior phenotyping of three months old wild-type and *Mecp2*$^{308/y}$ mice, treated with vehicle or TBA. Open field: Locomotor activity (travelled distance) and number of rears in the whole arena (top), and percentage of time spent in the center of the open field (bottom) during the 30 min habituation. Data are expressed as mean ± SEM and analyzed using two-way ANOVA. Bars represent mean +/- SEM.

Fig. 3 Morris water maze. Latency and distance to locate the hidden platform, percentage of time spent in the different quadrants and the number of platform position crosses during the probe trial. Data are expressed as mean ± SEM and analyzed using 3 factor repeated measures ANOVA. Data are expressed as mean ± SEM (bars and lines) together with scattergrams (preference and platform crosses) and analyzed using two or three-way ANOVA.

Fig. 4 Elevated plus maze: percentage of entries and percentage of time in the open arms, and number of closed arm entries. Data are expressed as mean ± SEM and analyze using two-way ANOVA.

Fig. 5 Marble burying: Percentage of 2/3 covered marbles. Data are expressed as mean ± SEM and analyzed using two-way ANOVA followed by Tukey's multiple comparisons test. **** p<0.0001 vs WT in the same treatment; ## p<0.01 vs Vehicle in the same genotype.

Fig. 6 Mecp2 deficiency decreases the ratio of acetylated to total tubulin in brain tissues (a, hippocampus; b, amygdala). Ratio of acetylated tubulin to β-III-tubulin (total tubulin) was significantly decreased as a result of Mecp2 deficiency (KO). The acetylated/total tubulin ratio increased after TBA treatment with WT and KO becoming statistically indistinguishable. * p<0.05. Western blot of acetylated alpha-tubulin and tubulin in the hippocampus (c) and in the amygdala (d) of wild type (WT) and KO *Mecp2* $^{308/y}$ mice treated with vehicle (-) or tubastatin A (TBA) (+).

Fig. 7 Quantification of mRNA *Hap1* levels in 17-weeks Mecp2-deficient brains using quantitative PCR (a: Amygdala; b: Hippocampus). Data are expressed as mean ± SEM and analyze using two-way ANOVA. * p<0.05

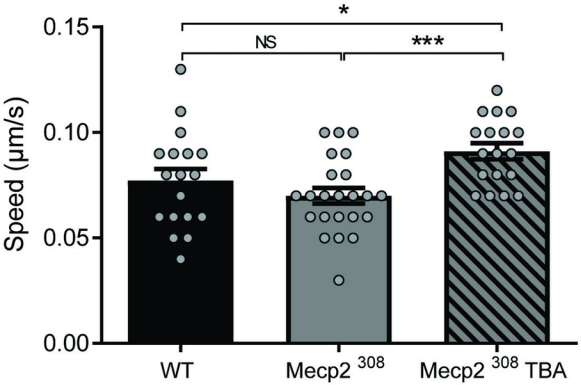
Speed (µm/s)
0.15
0.10
0.05
0.00
*
NS
***
WT
Mecp2 308
Mecp2 308 TBA

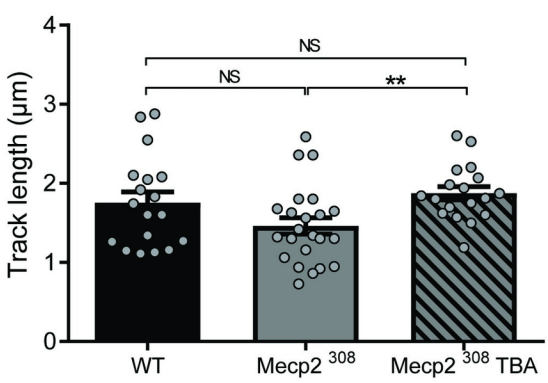
Track length (µm)
4
3
2
1
0
NS
NS
**
WT
Mecp2 308
Mecp2 308 TBA

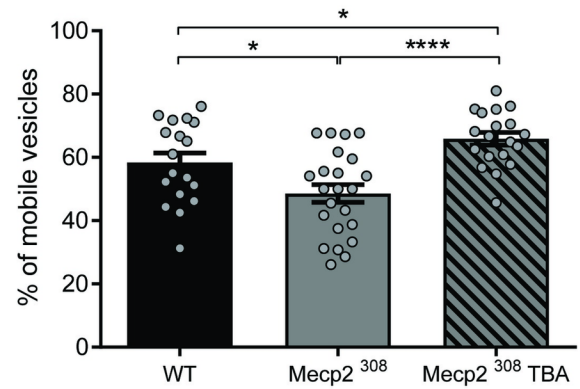
% of mobile vesicles
100
80
60
40
20
0
*
*
****
WT
Mecp2 308
Mecp2 308 TBA

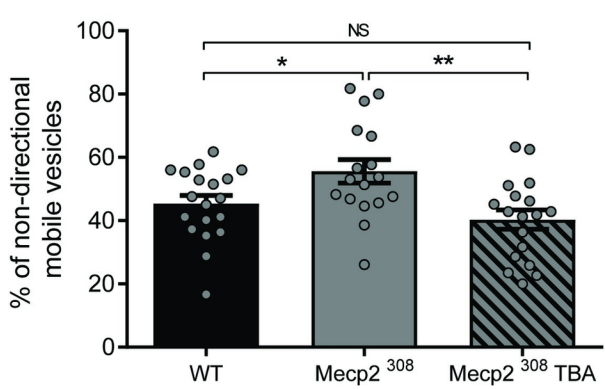
% of non-directional mobile vesicles
100
80
60
40
20
0
NS
*
**
WT
Mecp2 308
Mecp2 308 TBA

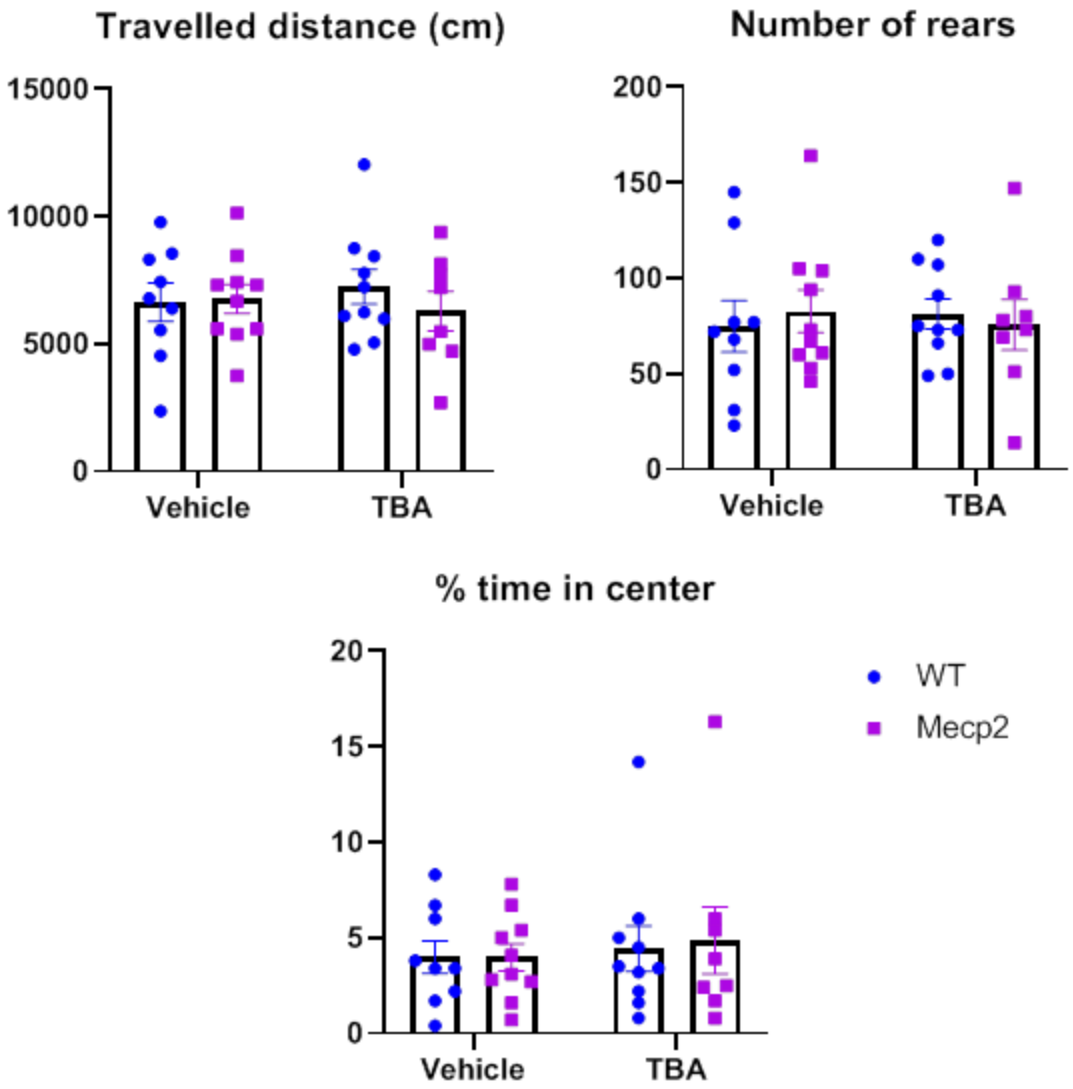
Travelled distance (cm)
15000
10000
5000
0
Vehicle
TBA
Number of rears
200
150
100
50
0
Vehicle
TBA
% time in center
20
15
10
5
0
Vehicle
TBA
WT
Mecp2

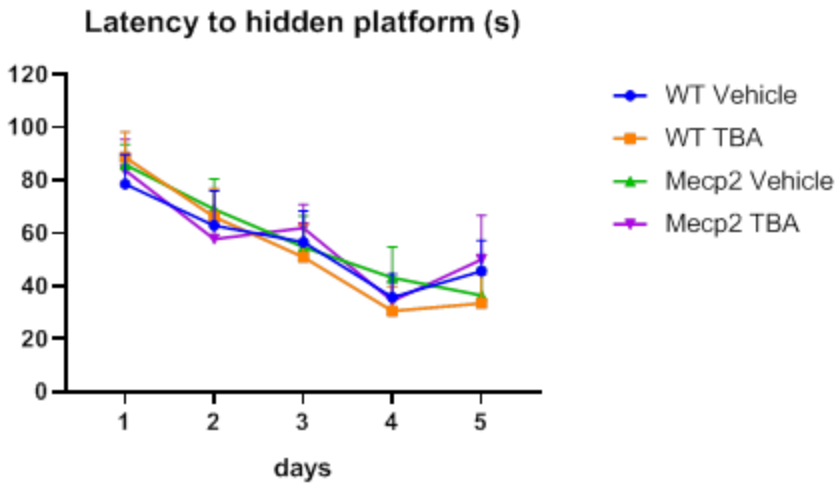
Latency to hidden platform (s)
120
100
80
60
40
20
0
1
2
3
4
5
days
WT Vehicle
WT TBA
Mecp2 Vehicle
Mecp2 TBA

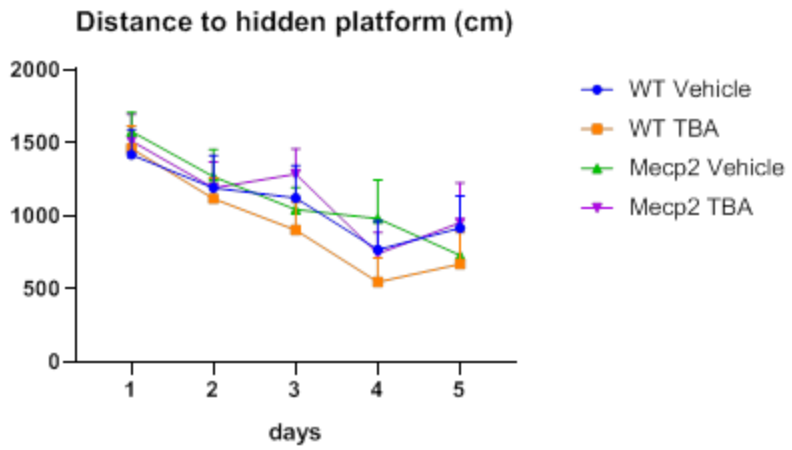
Distance to hidden platform (cm)
2000
1500
1000
500
0
1
2
3
4
5
days
WT Vehicle
WT TBA
Mecp2 Vehicle
Mecp2 TBA

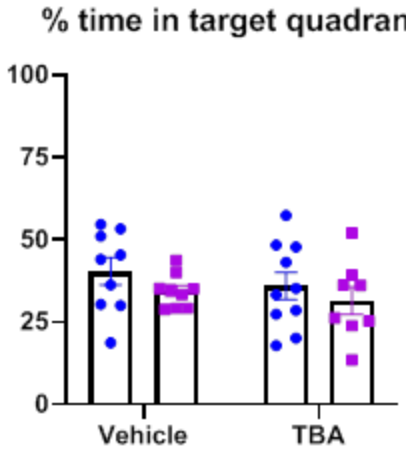
% time in target quadrant
100
75
50
25
0
Vehicle
TBA

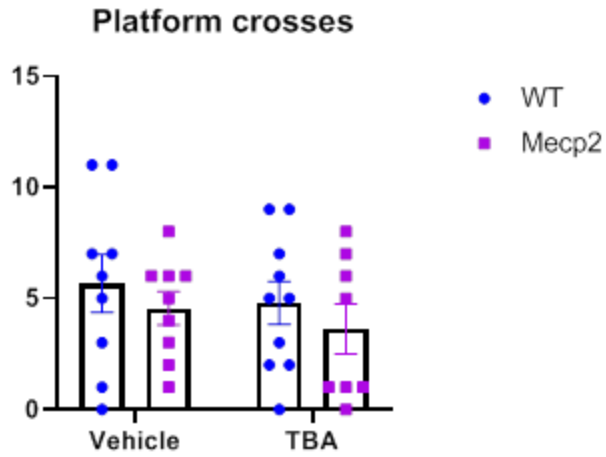
Platform crosses
15
10
5
0
Vehicle
TBA
WT
Mecp2

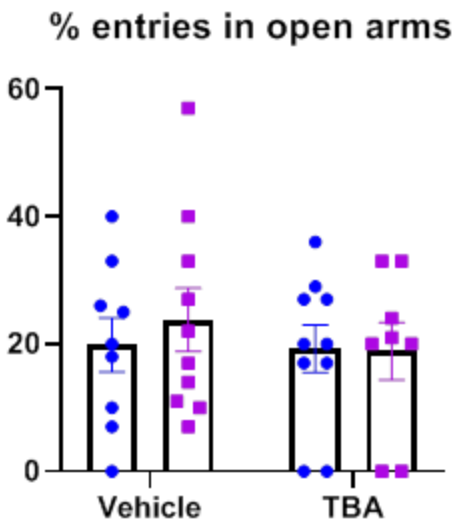
% entries in open arms
60
40
20
0
Vehicle
TBA

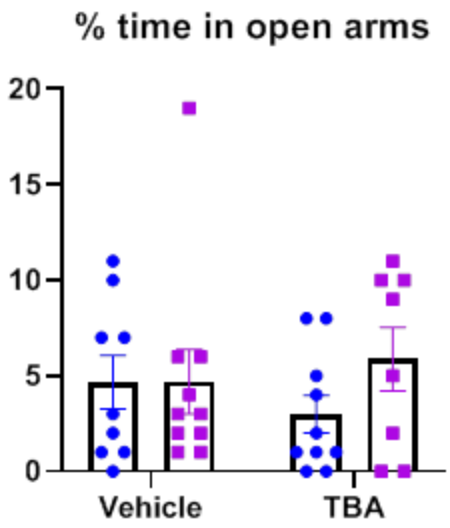
% time in open arms
20
15
10
5
0
Vehicle
TBA

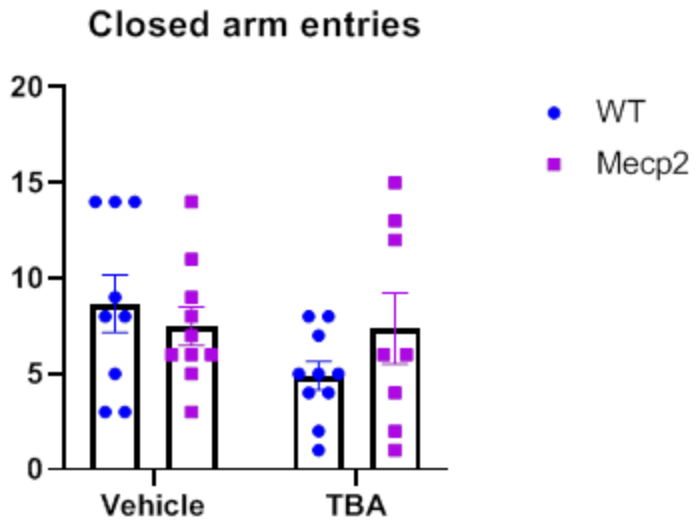
Closed arm entries
20
15
10
5
0
Vehicle
TBA
WT
Mecp2

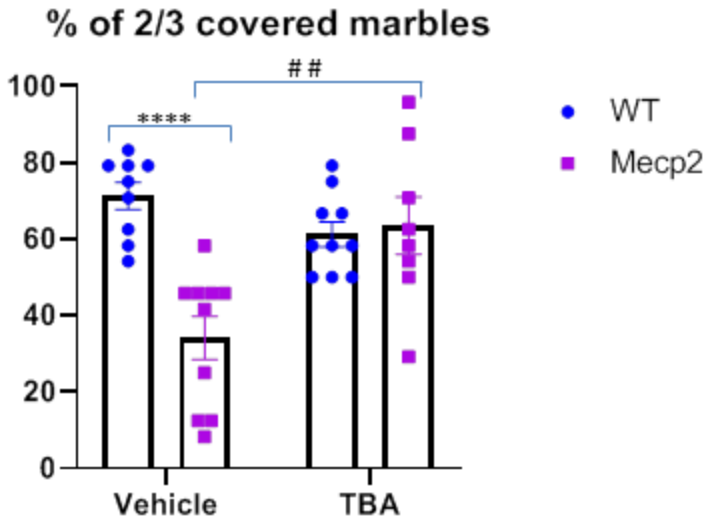
% of 2/3 covered marbles
##
****
100
80
60
40
20
0
Vehicle
TBA
WT
Mecp2

a.

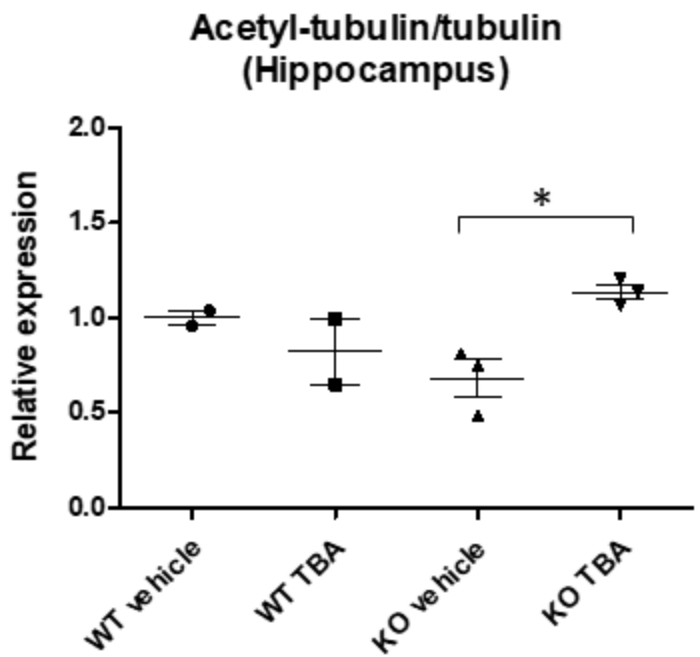
Acetyl-tubulin/tubulin
(Hippocampus)
Relative expression
2.0
1.5
1.0
0.5
0.0
*
WT vehicle
WT TBA
KO vehicle
KO TBA

b.

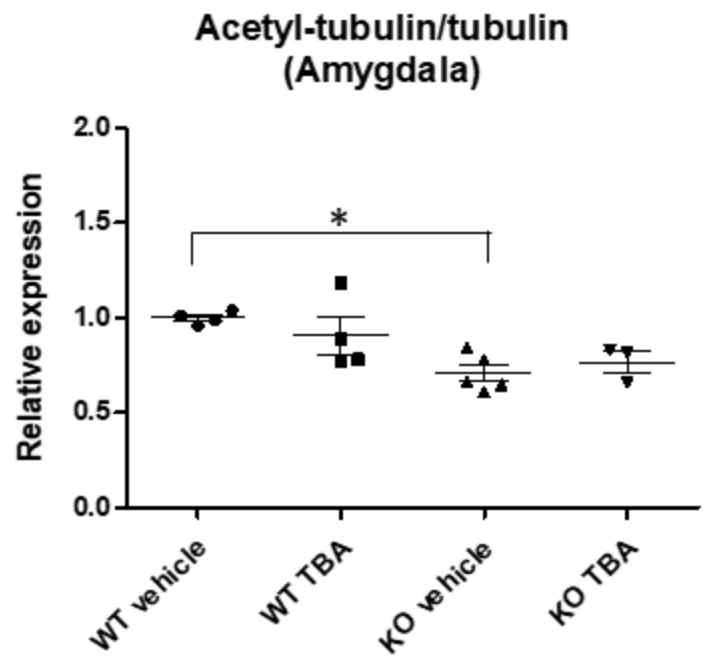
Acetyl-tubulin/tubulin
(Amygdala)
Relative expression
2.0
1.5
1.0
0.5
0.0
*
WT vehicle
WT TBA
KO vehicle
KO TBA

c.

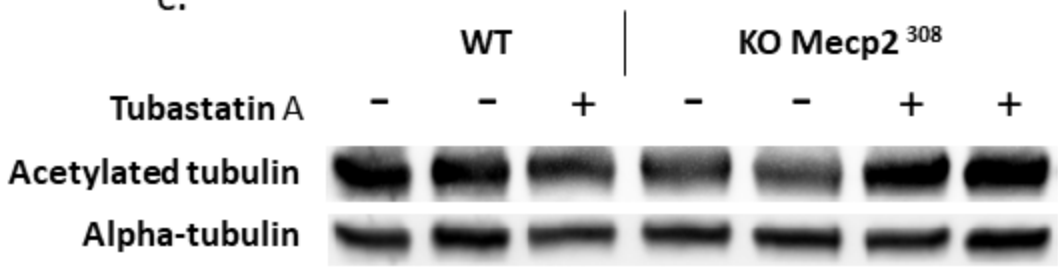
WT
KO Mecp2 308
Tubastatin A
- - + - - + +
Acetylated tubulin
Alpha-tubulin

d.

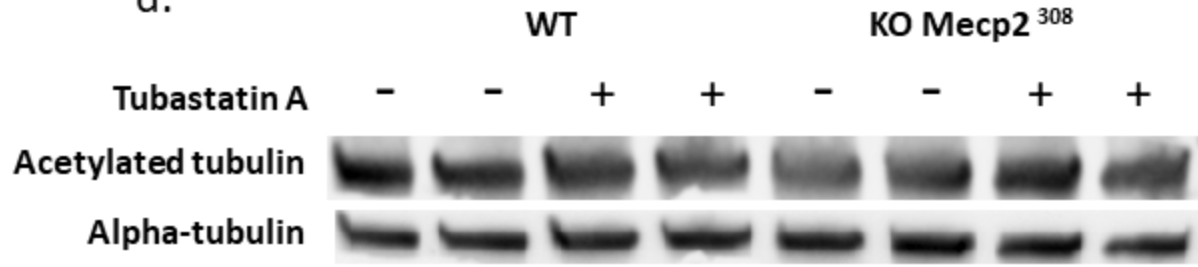
WT
KO Mecp2 308
Tubastatin A
- - + + - - + +
Acetylated tubulin
Alpha-tubulin

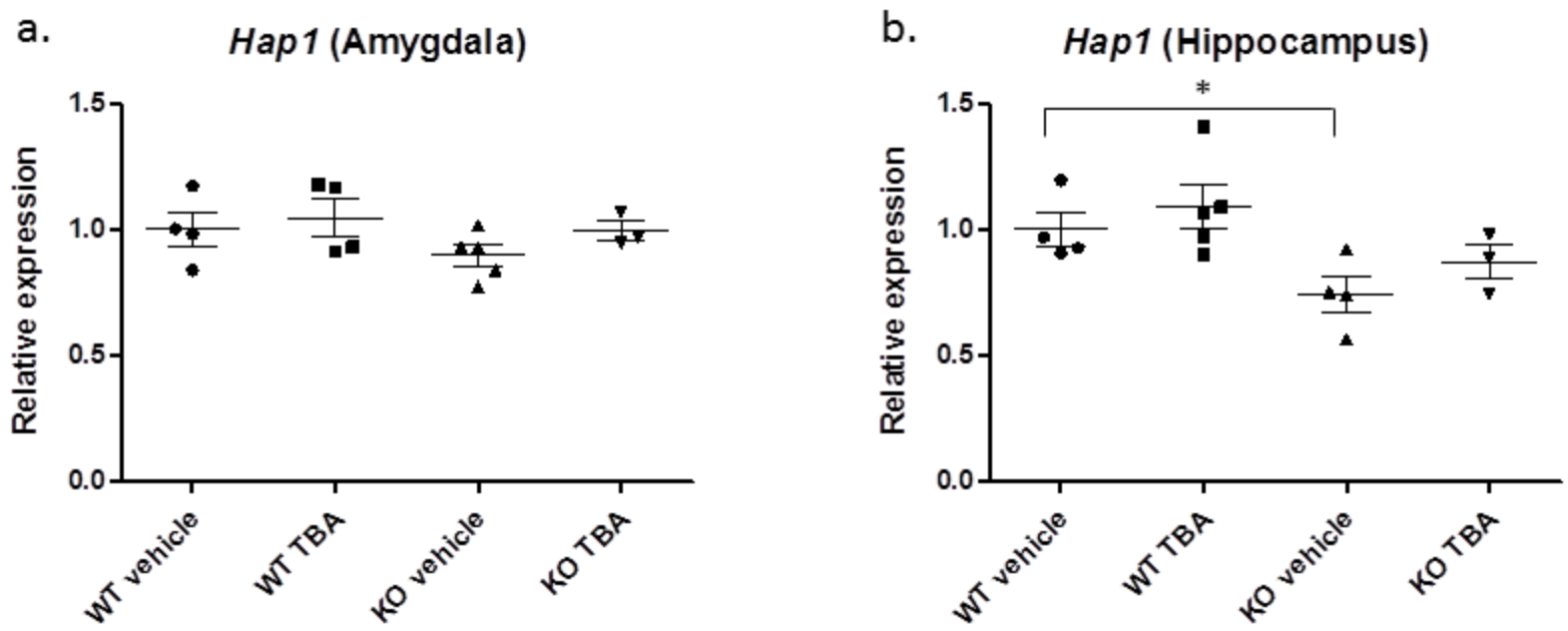
a.
Hap1 (Amygdala)
Relative expression
1.5
1.0
0.5
0.0
WT vehicle
WT TBA
KO vehicle
KO TBA
b.
Hap1 (Hippocampus)
*
Relative expression
1.5
1.0
0.5
0.0
WT vehicle
WT TBA
KO vehicle
KO TBA